J. Fluid Mech. (2004), *vol.* 510, *pp.* 95–104. © 2004 Cambridge University Press
DOI: 10.1017/S0022112004009590 Printed in the United Kingdom

Topographic advection of dense bottom water

By A. K. WÅHLIN

Oslo University, Department of Geophysics, Pb. 1022 Blindern, 0315 Oslo, Norway
awahlin@geofysikk.uio.no

(Received 23 October 2003 and in revised form 31 March 2004)

The time development of a dense eddy placed on a varying topography in a rotating system is the subject of this paper. It is shown that if the bathymetric variations are comparable with the thickness of the eddy, these will induce a first-order time development in the water mass. Large-amplitude geostrophic theory shows that the water is advected along the depth contours with a speed that is proportional to the slope of the bottom. The results are applied to a laboratory experiment with a rotating parabolic channel. According to theory, an initially circular eddy placed in the centre of the channel becomes elliptical while shifting its axis along the channel. The outcome of the experiment is in accordance with theory, and the importance of topographic advection in the ocean is discussed. It is suggested that the mechanism may be important for moving water from deep-water formation sites and into the global deep-water circulation.

1. Introduction

The subject of this paper is the time development of a purely geostrophic water mass as it flows over a varying topography. Since the velocity normal to the bottom is zero, the fluid converges where the flow is directed towards shallower topography and diverges where it is directed towards deeper topography. If the lateral boundaries are free then fluid is continuously relocated within the water mass as a result of this convergence and divergence.

On a sloping plane the relocation of fluid makes it translate parallell to the depth contours, with deep water to the left (in the Northern Hemisphere), at a constant velocity u_N. The shape of the water mass, and associated geostrophic velocities, does not affect the motion of the structure. Circular eddies of different size (Nof (1984)) as well as the leading edge of a continuous dense bottom current (Tyler & Kæse 2001; Wåhlin 2002) move with the same speed, which is proportional to the slope of the bottom and the reduced gravity, and inversely proportional to the Coriolis parameter.

The novel aspect presented here is that this mechanism – topographic advection – governs the flow also if the slope varies continuously underneath the water mass. The translation speed is still proportional to the slope of the bottom, but no longer a constant. This means that the water will move away along the topography in the regions where the bottom slopes, even though it is not forced or pumped in any way. A geostrophic dense water mass cannot remain stationary if it occupies a region where the bottom slopes. Its shape will change as portions of it moves along the depth contours. Again, it is the shape of the bottom that determines the time development and not the shape of the water mass (and associated geostrophic velocities). If the bathymetric variations are comparable in magnitude to the thickness of the fluid then this 'topographic advection' is a first-order effect.

https://doi.org/10.1017/S0022112004009590 Published online by Cambridge University Press

On a flat bottom there is no topographic advection and no first-order time-dependence, a consequence of what is sometimes called 'geostrophic degeneracy' (see e.g. Pedlosky 1987, chapter 2.10). The term refers to the fact that there is then a stationary geostrophic velocity field corresponding to each pressure distribution. The time dependence observed in a geostrophic flow on a flat topography is caused by higher-order dynamics, i.e. the ageostrophic effects induced either by friction or inertial acceleration. Accordingly a dense circular eddy spreads symmetrically under the influence of bottom friction (Gill *et al.* 1979; see also Huppert 1982), while the inertial accelerations induce baroclinic instabilities at the edges of the eddy. The instabilities grow in dense eddies on a flat bottom (Saunders 1973) as well as bouyant eddies in a denser environment (Griffiths & Linden 1981), and are also observed when the eddy is created by a constant flux of water from a localized source (Griffiths & Linden 1981) or by cooling of water from above (e.g. Jacobs & Ivey 1998; Legg & Marshall 1993).

The formation of deep western boundary currents are traditionally described as an outflow from some upstream basin filled with dense water (see e.g. Lane-Serff & Baines 1998; Jungclaus & Backhaus 1994; Price & Baringer 1994; Whitehead 1998). The present investigation suggests that an alternative mechanism may also be important in the ocean. When a dense water mass is placed on a sloping topography it will move forward, regardless of any pumping or forcing from adjacent basins. If water is cooled over a sloping topography the cold water moves away from the formation site, eventually shaping into a continuous current along the slope if the cooling continues long enough.

The large-amplitude geostrophic equations (Swaters 1991) are solved analytically for a 1.5-layer system in a parabolic channel. According to theory an initially circular distribution of dense water, placed in the centre of the channel, deforms into an ellipse that becomes more and more elongated with time, while gradually shifting its major axis. The solution is compared to a laboratory experiment in which a 'blob' of dense water is released in the centre of a rotating channel with parabolic bottom. Several experiments, in which a fixed volume of salt water was injected through a hole in the bottom of the tank, were conducted with varying salinity, rotation rate and two different topographies. The experiments agree qualitatively well with the theory. However bottom friction clearly influence the experiments in a quantitative sense, and the observed interface was more level and the water mass more spread out across the channel than expected from the (non-viscous) theory.

2. Theory

In figure 1 a dense current flowing over a smooth topography is shown together with the coordinate system and the notation used. The dense water is assumed to be well-mixed and underlying an infinitely deep fluid at rest. The density of the lower layer is ρ, its thickness h, and it is placed on a bathymetry with bottom elevation $D(x)$. Provided the flow is in geostrophic balance the horizontal velocities (u, v) in the (x, y) directions are given by

$$fu = -g' \frac{\partial h}{\partial y}, \quad -fv = -g' \left(\frac{\partial h}{\partial x} + \frac{\partial D}{\partial x} \right) \qquad (2.1a, b)$$

where f is the Coriolis parameter and $g' = g(\rho - \rho_0)/\rho_0$ is the reduced gravity (ρ_0 denoting the ambient fluid density). Inserting (2.1*a*, *b*) into the vertically integrated

https://doi.org/10.1017/S0022112004009590 Published online by Cambridge University Press

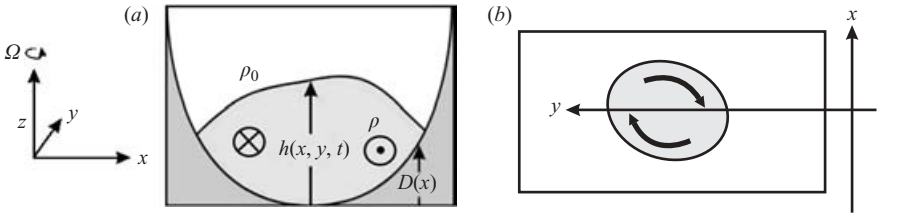

FIGURE 1. Sketch of a dense water mass on a smooth topography, together with the coordinate system and notation used. The arrows indicate the direction of the geostrophic flow. (*a*) Side view. (*b*) Top view.

continuity equation gives

$$\frac{\partial h}{\partial t} + \frac{g'}{f}\frac{\partial D}{\partial x}\frac{\partial h}{\partial y} = 0. \tag{2.2}$$

Solutions to (2.2) can be written as

$$h(t, x, y) = F(\eta)G(x), \tag{2.3a}$$

$$\eta = tu_N - y, \;\; u_N = \frac{g'}{f}\frac{\partial D}{\partial x}. \tag{2.3b}$$

The functions $F(\eta)$ and $G(x)$ are determined from the initial shape of the water mass. On a level topography, $\partial D/\partial x = 0$ and the distribution of h is stationary as a first-order description. However, when the bottom is not level the first-order solution is time dependent and the water is advected along the depth contours with speed u_N.

An initially circular eddy will evolve according to

$$h(x, y, t) = h_0\left(1 - \frac{\eta^2}{L_B^2} - \frac{x^2}{L_B^2}\right) \tag{2.4}$$

where η is given by (2.3*b*), L_B is the initial radius and h_0 is the initial maximum thickness.

In figure 2 the time development of (2.4) is shown as a function of x and y for a parabolic channel,

$$D(x) = \alpha x^2 \tag{2.5}$$

where $\alpha = 5.5\ \mathrm{m}^{-1}$.

The originally circular 'blob' changes shape and becomes more elliptical with time. The elongation varies according to the channel geometry and the ratio g'/f. As can be seen from (2.3) and (2.4) the blob would remain circular if plotted in an (η, x) plane. Looking into the channel from the side, several cross-sections will be visible simultaneously. Some of these are shown in the upper panels of figure 2. All cross-sections are members of the family of curves with envelope given by the centre section at $t = 0$. If infinitely many cross-sections were drawn, the structure would appear not to evolve in time.

3. Experiment set-up and results

Figure 3 shows a sketch of the experiment set-up. A rectangular tank of (inner) width 0.28 m, length 0.73 m and height 0.45 m was used. On each long sidewall, two straight groves were cut at 8 cm and 15 cm above the tank bottom. By sliding rectangular pieces of thin Plexiglas into the groves two different parabolic channel

https://doi.org/10.1017/S0022112004009590 Published online by Cambridge University Press

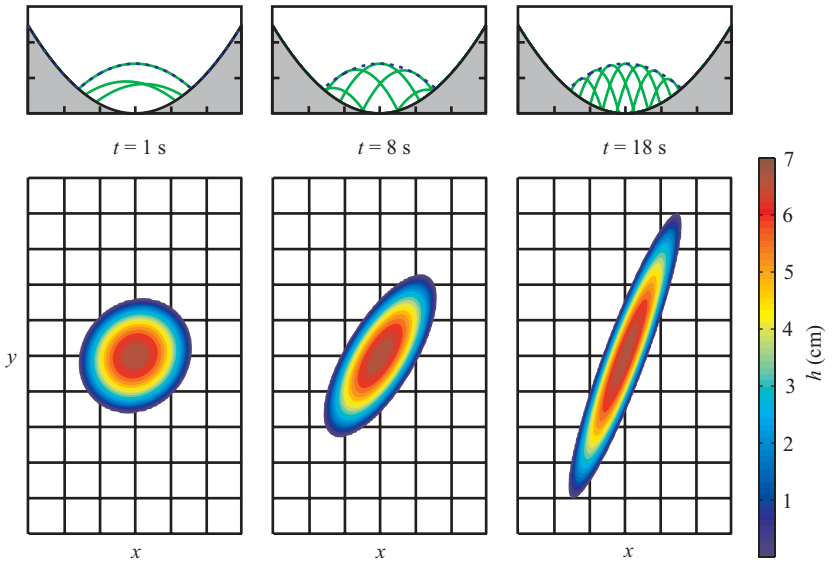

FIGURE 2. Time development of a 'blob' of dense water as calculated from (2.4) with parabolic topography $D(x) = \alpha x^2$ (where $\alpha = 5.5\ \mathrm{m}^{-1}$), $g' = 0.73\ \mathrm{cm\,s}^{-2}$ and $f = 0.63\ \mathrm{s}^{-1}$. Upper plots: Side view with cross-sections taken at every 5 cm. The dashed blue line shows the cross-section at $t = 0$ and $y = 0$. Lower plots: Top view with colours corresponding to thickness of the dense layer according to legend. Distance between background lines is 5 cm.

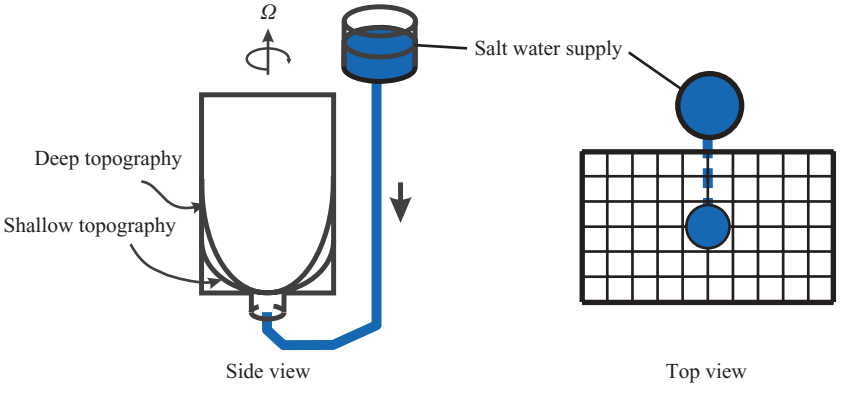

FIGURE 3. Sketch of the experiment set-up.

geometries were created – a shallow one with $\alpha \sim 3.7\,\mathrm{m}^{-1}$ and a deeper one with $\alpha \sim 5.5\,\mathrm{m}^{-1}$ (α pertaining to the curvature in (2.5)). In the centre of the channel a cylinder was fitted to a hole (of diameter 7.6 cm) in the bottom. The cylinder was filled with foam and connected to the salt water supply. The tank was filled with fresh water, spun up, and videotaped from above and from the side as a 'blob' of salt water was released through the cylinder.

By adjusting the rotation rate and the salinity of the salt water a series of experiments with different values of $g'$and f were performed for the two topographies. A fixed volume V of dense fluid was released through the hole in the bottom, after which the valve to the salt water was closed. The flow rate was adjusted for each experiment in order to obtain a quick release without too much mixing. Table 1 shows

https://doi.org/10.1017/S0022112004009590 Published online by Cambridge University Press

(*a*) g' (cm s^{-2})	0.37	0.37	0.73	0.73	1.1	1.1	1.5	1.5	1.9	1.9	2.2	2.2
f (s^{-1})	0.84	0.63	0.84	0.63	0.84	0.63	0.84	0.63	0.84	0.63	0.84	0.63
V (l)	0.8	0.8	0.9	0.9	0.9	0.9	0.8	1.0	0.9	0.9	0.8	0.8
Δt (s)	10	10	10	10	8	8	8	8	6	6	5	5
$\tau_N = f/(2g'\alpha)$ (s)	30	23	15	11.5	10	8	8	6	6	5	5	4
$\theta = g'h/(f^2L_B^2)$	0.04	0.06	0.07	0.13	0.11	0.19	0.15	0.26	0.18	0.32	0.22	0.39
$\tau' = \Delta t/\tau_N$	0.33	0.44	0.66	0.87	0.8	1	1	1.33	1	1.2	1	1.2
(*b*) g' (cm s^{-2})	0.37	0.37	0.73	0.73	1.1	1.1	1.5	1.5				
f (s^{-1})	0.84	0.63	0.84	0.63	0.84	0.63	0.84	0.63				
V (l)	0.9	0.8	1.1	1.1	0.9	1.0	0.9	0.8				
Δt (s)	10.5	10	9	7	8	8	8	8				
$\tau_N = f/(2g'\alpha)$ (s)	21	16	10	8	7	5	5	4				
$\theta = g'h/(f^2L_B^2)$	0.04	0.07	0.07	0.13	0.11	0.20	0.15	0.26				
$\tau' = \Delta t/\tau_N$	0.5	0.62	0.9	0.85	1.14	1.6	1.6	2.0				

TABLE 1. Experiment parameters. The topographic timescale τ_N is the time at which the major axis of the ellipse makes a 45 degree angle to the centreline, θ is the square of the width of the flow compared to the Rossby radius (based on width 10 cm and thickness 7 cm), and τ' is the ratio between the release time and τ_N. (*a*) Shallow topography ($\alpha = 3.7\,\mathrm{m}^{-1}$), (*b*) deep topography ($\alpha = 5.5\,\mathrm{m}^{-1}$).

a list of the parameter values for each experiment together with Δt, the time taken to release the volume V.

As the dense fluid oozed up through the cylinder it started to rotate, shaping into a dense anticyclonic eddy on the bottom of the tank. This eddy was wide compared to the Rossby radius for all model runs (table 1), and small-scale shear instabilities could be observed initially. As the topography began to affect the flow and the eddy deformed, the instabilities were suppressed and a stable circulation developed.

Figures 4 and 5 show a time-series of photographs from an experiment with the deep topography ($\alpha = 5.5\,\mathrm{m}^{-1}$). The time development can be compared to that of figure 2 that pertains to the same parameters. The time development of the laboratory 'blob' is basically in line with the theory, but there are clearly at least quantitative differences. For example the dense interface is not stationary when viewed from the side, and also the observed ellipse is wider than the theoretical one. Three mechanisms that were ignored in the simplified theory stand out as most likely candidates for causing the discrepancy, namely (i) bottom friction (ii) the initialization, and (iii) the centrifugal force.

(i) The timescale τ_D after which diffusive Ekman smoothing becomes important is $\tau_D = L_B^2 f/(g'\delta)$ (where δ is the Ekman layer thickness) – several minutes for the example shown in figure 4 (for $L_B = 0.1$ m and $\delta = 1$ mm). However, if the lateral boundaries slump, then these quickly move up or down the slope in order to make the interface horizontal (Wåhlin & Walin 2001). The relevant timescale for this process is $\tau_B = \tau_D\delta/h_0$ (where h_0 is the thickness of the fluid), or about 12 s (using $h_0 = 5$ cm). The adjustment can be seen clearly in figure 4. After 17 s the interface appears almost horizontal when viewed from the side, although the bulk flow is still moving along the channel at that time (figure 5). The result of the frictional adjustment of the boundaries is to move fluid uphill (out from the channel centre) at the upper flow boundaries and downhill (towards the channel centre) at the lower, i.e. a widening of the ellipse.

https://doi.org/10.1017/S0022112004009590 Published online by Cambridge University Press

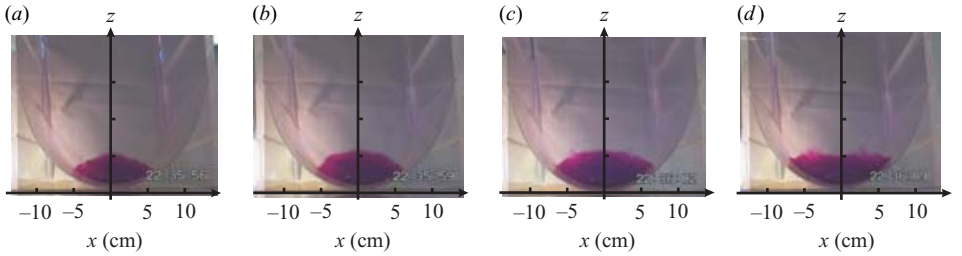

FIGURE 4. Side view photographs of the dense blob at times (*a*) $t = 3$ s, (*b*) $t = 7$ s, (*c*) $t = 10$ s, (*d*) $t = 17$ s. The experiment pertain to the deep topography with $\alpha = 5.5$ m^{-1}, $f = 0.63$ s^{-1} and $g' = 0.73$ cm s^{-2}. The distance between the notches on the centre lines are 5 cm.

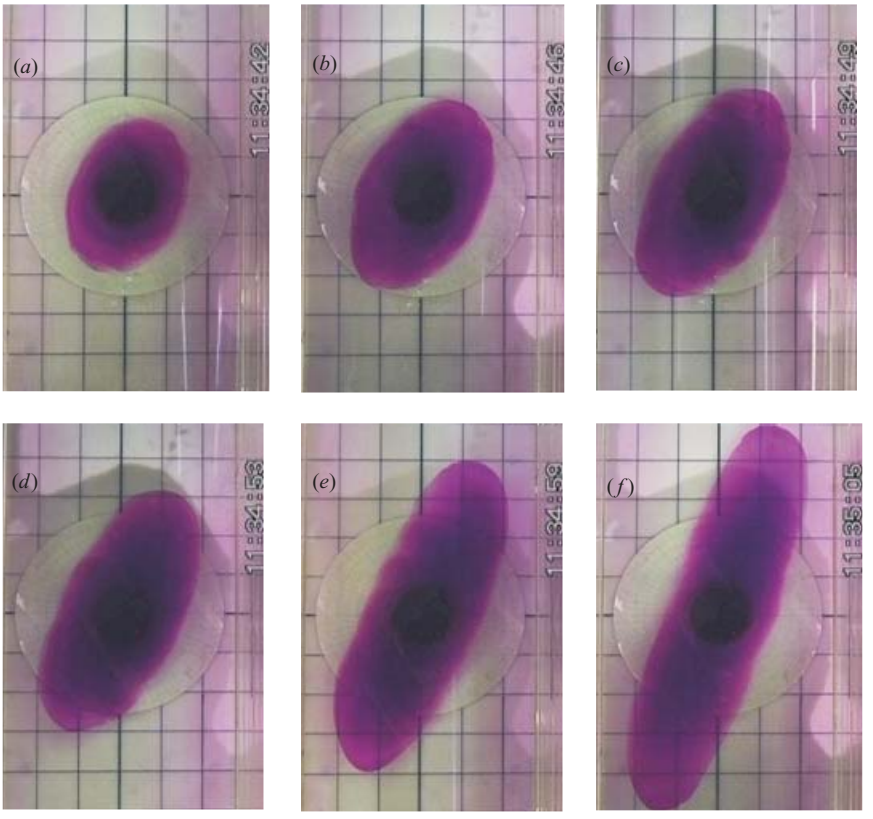

FIGURE 5. Top view photographs of the dense blob at times (*a*) $t = 1$ s, (*b*) $t = 5$ s, (*c*) $t = 8$ s, (*d*) $t = 12$ s, (*e*) $t = 18$ s, (*f*) $t = 24$ s. The experiment pertain to the deep topography with $\alpha = 5.5\,\mathrm{m}^{-1}$, $f = 0.63\,\mathrm{s}^{-1}$ and $g' = 0.73$ cm s^{-2}. The distance between the background lines is 5 cm.

(ii) Due to the release method there was a transition time of 5–10 s (see table 1) during which the connection to the salt water supply was open. As a consequence fluid was still being released when the topographic advection had started, resulting in a deformation of the elliptical shape. Table 1 shows the ratio τ' of the transition time and the topographic advection timescale τ_N defined as $\tau_N = f/(2g'\alpha)$, i.e. the time at which the major axis of the ellipse makes an angle 45° to the centreline of the channel. As can be seen they are comparable in magnitude.

https://doi.org/10.1017/S0022112004009590 Published online by Cambridge University Press

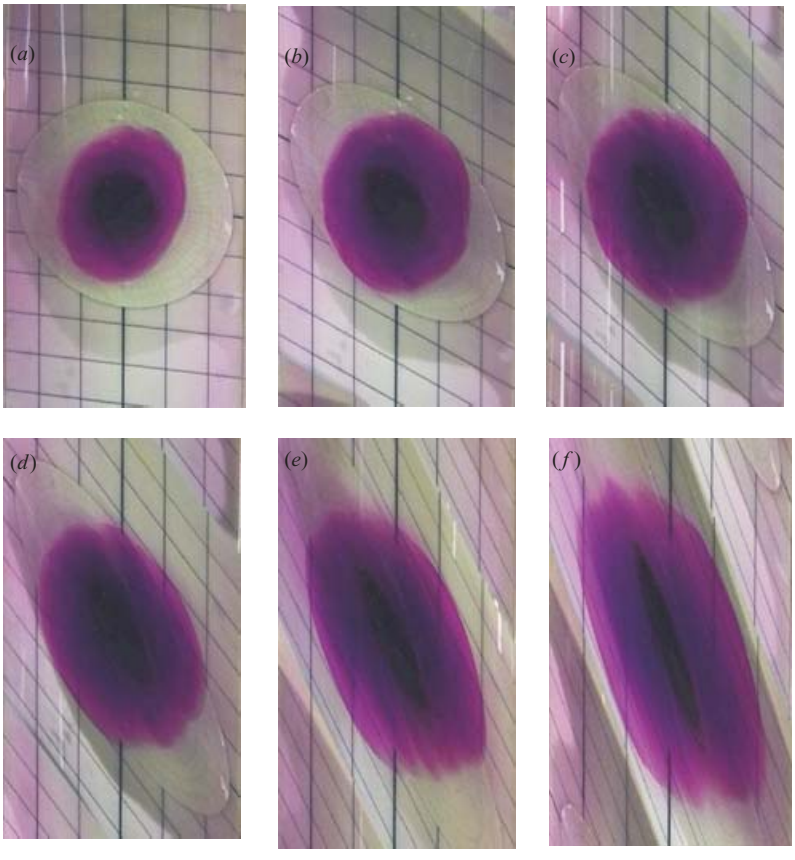

FIGURE 6. The same photographs as in figure 5, but translated and shown as a function of η and x, where $\eta = u_N t - y$ and $u_N = 2g'\alpha x/f$.

(iii) Because of the centrifugal force the potential surface is not horizontal, but a parabola. Although the additional slope is small in comparison with $\partial D/\partial x$, it imposes a slope of the channel axis. As was shown in Wåhlin (2002) water may be steered into a sloping channel. Consequently the sloping potential surface induces a motion towards the centreline in the experiments. The effect appears limited in the experiments reported here, but was visible in an additional set carried out with $f = 2.5\,\mathrm{s}^{-1}$.

Using (2.3) and (2.5) with $\alpha = 5.5\ \mathrm{m}^{-1}$, $f = 0.63\ \mathrm{s}^{-1}$ and $g' = 0.73\ \mathrm{cm\ s}^{-2}$, u_N (and thereby η) for each photo in figure 5 may be calculated as a function of x and y. This expression can be used to transform the photographs to an (η, x)-plane, which has been done in figure 6. According to theory the purple blob would remain a constant circular shape in the (η, x)-plane. The quantitative difference between the idealized theory and the experiment is evident in that the size of circle increases with time and that the circular shape is distorted for larger times.

Similar results were evident in all experiments. Figure 7 shows a summary of the complete experiment series, constructed by tracing (i.e. defining the boundary of the purple region with a bitmap tracing software) frames from the videotapes (*a*) before and (*b*) after transformation to the (η, x)-plane. The frames were grabbed at three different times corresponding to $\eta_1 = 0.2x - y$; $\eta_2 = 0.6x - y$; and $\eta_3 = 1.2x - y$.

https://doi.org/10.1017/S0022112004009590 Published online by Cambridge University Press

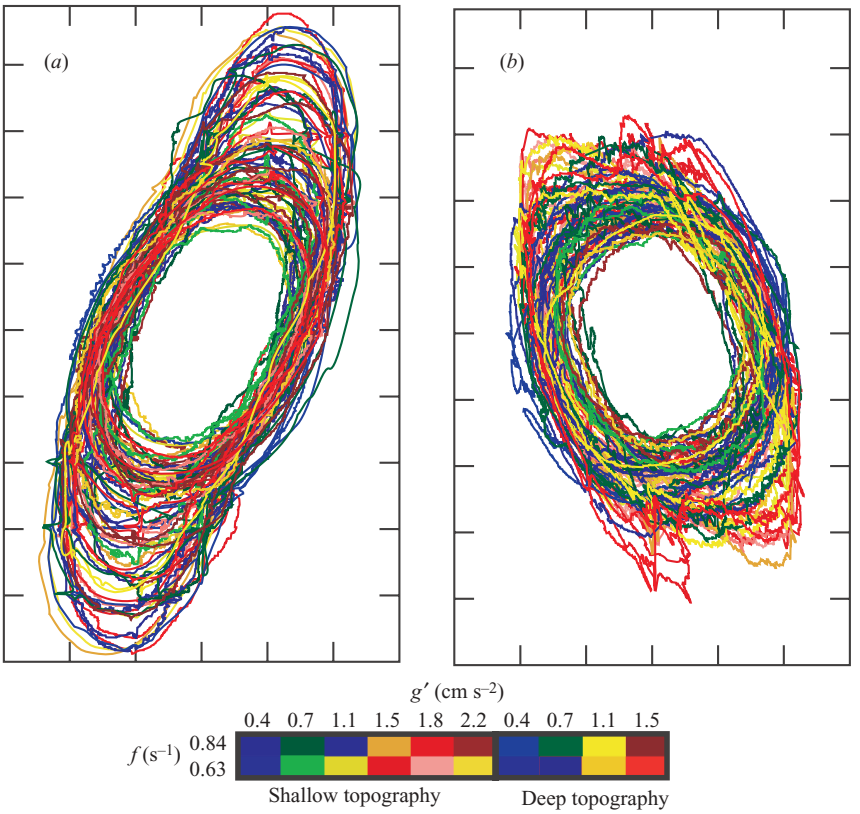

FIGURE 7. Summary of the complete experiment series. From each experiment three top-view pictures were chosen at times $t_1 = 0.1f/(g'\alpha)$; $t_2 = 0.3f/(g'\alpha)$; and $t_3 = 0.6f/(g'\alpha)$. The traced contours of each photograph are shown here as a function of (*a*) x and y and (*b*) x and η. The colours correspond to experiments according to legend, with blue and green shades for those in which the release mechanism was fast compared to the topographic advection and red/yellow when it was comparable in magnitude or slower.

The colours of the lines were chosen in order to distinguish between cases where the release of salt water was quick compared to the topographic advection.

4. Discussion

Isolated eddies that are larger than the Rossby radius, i.e. for which $\theta < 1$ (where $\theta = g'h/(f^2R^2)$, h is the thickness of the eddy and R is its radius), have a tendency to break up into or shed smaller eddies with radius comparable to the Rossby radius (see e.g. Saunders 1973; Griffiths & Linden 1981; Ivey 1987). The stability characteristics depend not only on θ but also on d, the ratio of the eddy thickness to the ambient fluid depth (Griffiths & Linden 1981). For $d \sim 1$ the eddy is stable for $\theta > 1.8$ (Saunders 1973) and the instability barotropic (Griffiths & Linden 1981), but for small d the instability is baroclinic and may be marginally stable for smaller θ (Griffiths & Linden 1981). In the present experiments $d \sim 0.1$, and the flow would be expected to be unstable for $\theta < 0.55$ (Griffiths & Linden 1981). Similar instabilities are also observed in convectively driven flows (see e.g. Jacobs & Ivey 1998; Legg & Marshall 1993) and as a stratified fluid is mixed locally to produce a homogeneus

https://doi.org/10.1017/S0022112004009590 Published online by Cambridge University Press

eddy (Ivey 1987). They play an important role in ocean circulation since they remove cooled water from its convection site (Marshall & Schott 1999).

The rate at which this mechanism transports water radially away from the centre may be estimated as the radius of the small eddies (of the same order of magnitude as the Rossby radius $\sqrt{g'h}/f$) divided by the time it takes for them to form (approximately 4–10 rotation periods). These observations pertain to both dense (Saunders 1973) and light (Griffiths & Linden 1981) eddies, although eddies with small d have slower radial motion (Griffiths & Linden 1981). Accordingly the velocity with which instabilities form and move out from the centre is less than, but comparable with, $\sqrt{g'h}/(20\pi)$. This velocity may be compared to that found by Jones & Marshall (1997) for the restratification after deep convection,

$$v_{restrat} = \sqrt{g'h}/56. \tag{4.1}$$

In the present experiments the topography varied underneath the dense eddy, and water was relocated by the topographic advection. Depending on the steepness of the topography, this mechanism may move the water at a much faster rate than that given by (4.1). As was shown in § 2 the fluid moves with the speed u_N. When compared to (4.1) it is seen that topographic advection removes water faster than the eddy-induced transport provided $\partial D/\partial x > \sqrt{h/g'}f/56$.

This is also confirmed by the present results (in which this criterion was well satisfied): no instabilities were observed even for the cases with $\theta \ll 0.55$ (see table 1), and topographic advection was clearly the dominant mechanism. However, in additional experiments with rotation period 5 s (not reported here) a tendency to break up into two water masses could be observed for flows having the same θ as the stable cases reported here. The process was slower (about 15 rotation periods) than expected from baroclinic instability and may also have been an effect of centrifugal forces in the along-channel direction.

The present results suggest that if a newly formed dense water mass of $g' = 0.5$ cm s^{-2}, that is 100 m thick and 100 km wide sinks to the bottom in a (high-latitude) region where the bottom slope is 0.01, then it will be gone from the formation site within a week. On a flat bottom (or if the water does not sink to the bottom) the same water mass would remain in the region for over a month.

If the salt-water supply is left open a continuous bottom current parallel to the bottom develops on each side of the channel (this was also observed in additional experiments not reported here). An alternative way of producing dense slope currents is to place a source of dense water on top of a slope (see Lane-Serff & Baines 1998 where a summary of earlier experiments is also given). Such flows are subject to vortex-stretching in the upper layer that may cause eddy formation (see also Swaters 1991). An important difference is that in the present work the dense water is in geostrophic balance at the bottom of the tank as it starts to advect along the slope. Hence there is no initial adjustment phase when the water flows downhill before it becomes geostrophic.

Although some oceanic outflows exit from narrow straits onto a slope, there are several locations where the strait gradually widens to a basin and the flow is in geostrophic balance. These might be better described by the present 'balanced' approach. For example the flow of dense water through sill-basin systems does not necessarily take the form of subsequent filling of each basin. Provided the flow is geostrophic it can propagate along the walls without filling the basin. It was shown by Mauritzen (1996) that a similar circulation prevails in the Nordic Seas. As the relatively warm and light Atlantic water cools it becomes denser than the

https://doi.org/10.1017/S0022112004009590 Published online by Cambridge University Press

surrounding water and sinks beneath the sea surface. It then flows anticlockwise along the topography and finally back into the Atlantic across the Greenland-Scotland ridge.

Perhaps the most interesting application of the present results is in global ocean circulation. It has been shown that the forward motion of a geostrophic dense water mass may be controlled by the sloping topography and not the forcing from the source. This means that the bathymetry of the ocean basins may be crucial for making the cold water formed at high latitudes move southward, and that there is a mechanism that constantly moves cold water from high to low latitudes.

This work was performed during a stay at the Department of Oceanography, Florida State University. Discussions with Professor D. Nof and tank-construction by Dave Oliff were much appreciated. I am also grateful for use of the laboratory facilities at the Geophysical Fluid Dynamics Institute and to Dr R. Kung, Ken Decoteau and Trond Kristiansen for technical assistance. The work was financed by the Kristine Bonnevie travel stipend, NSF grant 0241036 (to D. Nof) and NASA grant NAG10860 (to D. Nof), for which I am grateful.

REFERENCES

Gill, A. E., Smith, J. M., Cleaver, R. P., Hide, R. & Jonas, P. R. 1979 The vortex created by mass transfer between layers of a rotating fluid. *Geophys. Astrophys. Fluid Dyn.* **12**, 195–200.

Griffiths, R. W. & Linden, P. F. 1981 The stability of vortices in a rotating, stratified fluid. *J. Fluid Mech.* **105**, 283–316.

Huppert, H. E. 1982 The propagation of two-dimensional and axisymmetric viscous gravity currents over a rigid horizontal surface. *J. Fluid Mech.* **121**, 43–58.

Ivey, G. N. 1987 Boundary mixing in a rotating, stratified fluid. *J. Fluid Mech.* **183**, 25–44.

Jacobs, P. & Ivey, G. N. 1998 The influence of rotation on shelf convection. *J. Fluid Mech.* **369**, 23–48.

Jones, H. & Marshall, J. 1997 Restratification after deep convection. *J. Phys. Oceanogr.* **27**, 2276–2287.

Jungclaus, J. & Backhaus, J. 1994 Application of a transient reduced gravity plume model to the Denmark Strait Overflow. *J. Geophys. Res.* **99**, 12375.

Lane-Serff, G. F. & Baines, P. G. 1998 Eddy formation by dense flows on slopes in a rotating fluid. *J. Fluid Mech.* **363**, 229–252.

Legg, S. & Marshal, J. L. 1993 A heton model of the spreading phase of open-ocean deep convection. *J. Phys. Oceanogr.* **23**, 1040–1056.

Marshall, J. & Schott, F. 1999 Open-ocean convection: Observations, theory, and models. *Rev. Geophys.* **37**, 1–64.

Mauritzen, C. 1996 Production of dense overflow water feeding the North Atlantic across the Greenland-Scotland ridge. Part 1: Evidence for a revised circualtion scheme *Deep-Sea Res.* **43**, 769–806.

Nof, D. 1984 The translation of isolated cold eddies on a sloping bottom. *Deep-Sea Res.* **30**, 171–182.

Pedlosky, J. 1987 *Geophysical Fluid Dynamics*, 2nd Edn. Springer.

Price, J. F. & Baringer, M. O'N. 1994 Outflows and deep water production by marginal seas. *Prog. Oceanogr.* **33**, 161–200.

Saunders, P. M. 1973 The instability of a baroclinic vortex. *J. Phys. Oceanogr.* **3**, 61–65.

Swaters, G. E. 1991 On the baroclinic instability of cold-core coupled density fronts on a sloping continental shelf. *J. Fluid Mech.* **224**, 361–382.

Tyler, R. H. & Kæse, R. 2001 A string function for describing the propagation of baroclinic anomalies in the ocean. *J. Phys. Oceanogr.* **31**, 765–776.

Whitehead, J. 1998 Topographic control of oceanic flows in deep passages and straits. *Rev. Geophys.* **36**, 423–440.

Wåhlin, A. 2002 Topographic steering of dense water with application to submarine canyons. *Deep-Sea Res.* **49**, 305–320.

Wåhlin, A. & Walin, G. 2001 Downward migration of dense bottom currents. *Environ. Fluid Mech.* **1**, 257–279.

https://doi.org/10.1017/S0022112004009590 Published online by Cambridge University Press